

A Low-Rank Bayesian Approach for Geoadditive Modeling

Bryan Sumalinab^{*1,2}, Oswaldo Gressani¹, Niel Hens^{1,3}, Christel Faes¹

¹Interuniversity Institute for Biostatistics and statistical Bioinformatics (I-BioStat),
Data Science Institute (DSI), Hasselt University, Hasselt, Belgium

²Department of Mathematics and Statistics, College of Science and Mathematics,
Mindanao State University - Iligan Institute of Technology, Iligan City, Philippines

³Centre for Health Economic Research and Modelling Infectious Diseases (CHERMID),
Vaccine & Infectious Disease Institute, Antwerp University, Antwerp, Belgium

arXiv:2407.05854v1 [stat.ME] 8 Jul 2024

*Corresponding author. *E-mail address*: bryan.sumalinab@uhasselt.be

Abstract

Kriging is an established methodology for predicting spatial data in geostatistics. Current kriging techniques can handle linear dependencies on spatially referenced covariates. Although splines have shown promise in capturing nonlinear dependencies of covariates, their combination with kriging, especially in handling count data, remains underexplored. This paper proposes a novel Bayesian approach to the low-rank representation of geoadditive models, which integrates splines and kriging to account for both spatial correlations and nonlinear dependencies of covariates. The proposed method accommodates Gaussian and count data inherent in many geospatial datasets. Additionally, Laplace approximations to selected posterior distributions enhances computational efficiency, resulting in faster computation times compared to Markov chain Monte Carlo techniques commonly used for Bayesian inference. Method performance is assessed through a simulation study, demonstrating the effectiveness of the proposed approach. The methodology is applied to the analysis of heavy metal concentrations in the Meuse river and vulnerability to the coronavirus disease 2019 (COVID-19) in Belgium. Through this work, we provide a new flexible and computationally efficient framework for analyzing spatial data.

Keywords: Kriging, Geoadditive models, Bayesian P-splines, Laplace approximations, Low-rank model.

1 Introduction

Observations characterized by spatial locations often exhibit inherent correlations, with closer observations demonstrating stronger dependencies than those farther apart. This spatial correlation phenomenon is a fundamental aspect of spatial data analysis, especially in disciplines such as geostatistics, where the spatial arrangement of data points provides valuable insights into underlying processes where proximity often implies similarity. [Cressie \(1993\)](#) categorized spatial data into three main types: areal (or lattice) data, geostatistical (continuous) data, and point patterns. Our primary focus here is on the analysis of geostatistical data. Geostatistics is a field dedicated to studying phenomena that are continuously distributed over spatial domains. For example, in environmental studies, nearby soil samples are likely to have similar characteristics due to shared environmental conditions and geological processes. The principles and methodologies of geostatistics can also be applied to phenomena that are not strictly continuous (e.g. areal data), including those related to epidemic modeling and public health outcomes. For example, geostatistical methods can be used to assess the impact of spatially referenced exposure/covariates on health outcomes, model the spatial variation in disease incidence rates, identify high-risk areas, and assess the spatial dependence of disease transmission (see e.g. [Waller and Gotway, 2004](#); [Diggle and Giorgi, 2019](#)). In addition, spatial interpolation techniques, similar to those used in geostatistics, can also help to estimate disease prevalence in regions with sparse or missing data.

One of the primary applications in geostatistics is spatial prediction/interpolation, where missing or unobserved values at specific (unsampled) locations within a spatial domain are estimated. Kriging, a widely used geostatistical technique, relies on spatial correlations to interpolate and predict values across a spatial domain. Kriging methods estimate the spatial variability by considering the spatial arrangement and correlation between observations, resulting in predictions that minimize estimation errors. The strength of kriging lies in its ability to incorporate both the spatial trend and the spatial correlation structure of the data, making it a powerful tool

for spatial data analysis. Although theories about kriging are well established, dealing with larger sample sizes presents a significant computational burden, which is particularly evident in the inversion of the covariance matrix. The computational cost increases as the dimension of the covariance matrix grows with sample size. A promising solution comes in the form of low-rank representations of spatial models using basis functions, which substantially improve computation time. These low-rank approaches, reviewed by [Wikle \(2010b\)](#) and [Cressie et al. \(2022\)](#), offer a practical means to handle large datasets. One such low-rank kriging approach is proposed by [Kammann and Wand \(2003\)](#), and involves reducing the spatial locations with a subset, called “knots”, using a space-filling algorithm ([Johnson et al., 1990](#); [Nychka and Saltzman, 1998](#)). They adopt a spline-basis approach and rely upon the commonly used stationary covariance matrix in kriging as the basis functions. Their method offers not only computational advantages for handling big data but also ease of implementation through standard mixed models software. In addition to kriging, other techniques and modeling approaches are employed to address specific challenges and objectives. Generalized additive models ([Wood, 2017](#)), for instance, offer flexible frameworks for capturing nonlinear relationships in the data. This approach was also implemented by [Kammann and Wand \(2003\)](#) in combination with spatial smoothing, which they termed as geoaddivitive modeling. [Vandendijck et al. \(2017\)](#) extended their method by proposing to estimate the spatial decay parameter. Both approaches ([Kammann and Wand, 2003](#); [Vandendijck et al., 2017](#)) use likelihood-based estimation methods through mixed model representations of splines ([Wand, 2003](#); [Ruppert et al., 2003](#)) and are implemented in the context of Gaussian data.

This paper proposes a Bayesian approach for geoaddivitive modeling where spatial components are modeled in a similar way as in [Kammann and Wand \(2003\)](#). The Laplace approximation is used to approximate the posterior distribution of regression parameters, so as to significantly reduce the computational time to carry out inference as compared to traditional Markov chain Monte Carlo (MCMC) algorithms. Penalized B-splines (P-splines) ([Eilers and Marx, 1996](#)) are used to model the nonlinear effects of covariates. This smoother offers the advantage of a penalty matrix that can be easily constructed and naturally translated into a Bayesian framework ([Lang and Brezger, 2004](#)). The combination of Laplace approximations and P-splines (Laplacian-P-

splines) in generalized additive models developed by [Gressani and Lambert \(2021\)](#) offers a computationally efficient alternative to classic MCMC approaches and serve as a backbone to the methodology developed here. We extend the Laplacian-P-splines methodology to a geoaddivitive model. Additionally, a novel approach is proposed for handling count data in combination with linear and nonlinear dependencies on covariates, an aspect not well explored in the literature on geostatistical modeling. Typically, a Poisson distribution is assumed for count data. However, this assumption is inadequate for handling overdispersion, where the variability exceeds the mean, as the Poisson model requires the mean and variance to be equal. In contrast, the negative binomial distribution, although more complex, accounts for overdispersion and permits more sophisticated modeling of count data. This paper implements both Poisson and negative binomial distributions, providing a robust and flexible approach for handling spatial count data.

The article is organized as follows. Section 2 introduces the geoaddivitive model, explaining how the smooth covariates and spatial components are modeled. It also presents the Bayesian geoaddivitive model and discusses the use of Laplace approximations, optimization of hyperparameters, predictions, criteria for model selection, and hypothesis testing for the significance of nonlinear covariates. Section 3 conducts a simulation study to assess the proposed methodology using various performance measures, including bias, relative bias, and credible and prediction interval coverage. In Section 4, the proposed model is applied to the analysis of two real-world datasets: the Meuse river data and the coronavirus disease 2019 (COVID-19) vulnerability data in Belgium. Finally, Section 5 concludes the paper. Code to reproduce results of this article is available on the following repository <https://github.com/bryansumalinab/Geoaddivitive-Modeling.git>.

2 Important concepts and methodology

2.1 Geoaddivitive model

Consider spatially indexed observations denoted by $y_i(\mathbf{w}_i)$, where $\mathbf{w}_i = (w_{1i}, w_{2i})^\top \in \mathbb{R}^2$ denotes the spatial coordinates for $i = 1, \dots, n$. The observations $y_i(\mathbf{w}_i)$ are typically assumed to have a distribution from an exponential family as in generalized linear models. The geoaddivitive model

can be written as:

$$g(\mu_i) = \underbrace{\beta_0 + \beta_1 x_{i1} + \cdots + \beta_p x_{ip}}_{\text{Linear predictors}} + \underbrace{f_1(s_{i1}) + \cdots + f_q(s_{iq})}_{\text{Smooth terms}} + \underbrace{s(\mathbf{w}_i)}_{\text{Spatial component}}, \quad (1)$$

where $g(\cdot)$ is the link function and $\mathbb{E}(y_i(\mathbf{w}_i)) = \mu_i$. Model (1) consists of three different components. The first component contains the linear predictors $(1, x_{i1}, \dots, x_{ip})$, with corresponding parameters $(\beta_0, \beta_1, \dots, \beta_p)$. The second component captures nonlinear dependencies of $g(\mu_i)$ on covariates s_{ij} , for $j = 1, \dots, q$. Each smooth covariate s_{ij} can be modeled as:

$$f_j(s_{ij}) = \sum_{k=1}^K \theta_{jk} b_{jk}(s_{ij}), \quad j = 1, \dots, q,$$

where $b_{jk}(\cdot)$ is a basis function and θ_{jk} is the coefficient for $k = 1, \dots, K$. In our case, the B-spline basis function is used with a discrete difference penalty on successive B-spline coefficients proposed by [Eilers and Marx \(1996\)](#). The penalty controls the roughness of the fit and can be naturally extended to the Bayesian framework in formulating the joint prior distribution of the B-spline coefficients ([Lang and Brezger, 2004](#)). That is, if we let $\boldsymbol{\theta}_j = (\theta_{j1}, \theta_{j2}, \dots, \theta_{jK})^\top$, then a Gaussian prior distribution is assumed on $\boldsymbol{\theta}_j$ given by $(\boldsymbol{\theta}_j | \lambda_j) \sim \mathcal{N}_K(\mathbf{0}, (\lambda_j P)^{-1})$ where $\lambda_j > 0$ is the penalty parameter for the j th smooth model component and $P = D_m^\top D_m$ where D_m denotes the m th order difference matrix ($m = 2$ in this paper). To ensure that the penalty matrix is of full rank, a diagonal matrix is added to P with small entries on the main diagonal (e.g. 10^{-12}).

The third component of (1), $s(\mathbf{w}_i)$, accounts for spatial correlation and can be modeled in several ways depending on the type of spatial data. In kriging or classical geostatistics, the observations $y_i(\mathbf{w}_i)$ are assumed to be continuous in the spatial domain \mathbf{w}_i , and $s(\mathbf{w}_i)$ is assumed to be a Gaussian process with mean 0 and variance σ_w^2 . An important assumption of kriging is that $s(\mathbf{w}_i)$, for $i = 1, \dots, n$, are correlated such that $\text{Cov}(s(\mathbf{w}_i), s(\mathbf{w}_j)) = R(\mathbf{w}_i - \mathbf{w}_j)$, which satisfies the stationarity assumption since the covariance function $R(\cdot)$ only depends on the distances between spatial locations. The main goal of kriging is to predict observations at a given location. For Gaussian data, the best linear unbiased prediction for an arbitrary location is analytically available along with the corresponding prediction uncertainty ([Zimmerman and](#)

Stein, 2010). For non-Gaussian data, one can rely, for example, on Bayesian (Wikle, 2010a) or likelihood-based methodologies (Zimmerman, 2010).

Kriging predictions require to compute the inverse of the covariance matrix $R(\cdot)$ which is of dimension $n \times n$. With increasing sample size, the computational burden associated to these predictions becomes non-negligible. One way to address this problem is to write the spatial component in terms of the basis function model as follows:

$$s(\cdot) = \sum_{l=1}^L \alpha_l b_l(\cdot) + \varepsilon, \quad (2)$$

where $b_l(\cdot)$ is a known basis function and α_l are the coefficients for $l = 1, \dots, L$ with $L < n$. Define $\boldsymbol{\alpha} = (\alpha_1, \dots, \alpha_L)^\top$. The vector $\boldsymbol{\alpha}$ is assumed to have a multivariate Gaussian distribution, that is, $\boldsymbol{\alpha} \sim \mathcal{N}_L(0, \Sigma_{\boldsymbol{\alpha}})$ where the form of $\Sigma_{\boldsymbol{\alpha}}$ depends on the choice of the basis function and the error term ε is usually assumed to have a Gaussian distribution with mean 0 and constant variance. The addition of the error term ε accounts for the errors stemming from approximating the underlying spatial process with a finite set of basis functions or its low-dimensional representation (Wikle, 2010b; Cressie et al., 2022). Several choices can be made for the basis functions. One such choice is the method proposed by Kammann and Wand (2003) using the stationary covariance function in kriging as the basis function. By replacing the coordinates by a set of points, called knots, this approach allows for a low-rank representation of the covariance function. The spatial component $s(\mathbf{w}_i)$ is modeled as follows:

$$s(\mathbf{w}_i) = \beta_{w_1} w_{1i} + \beta_{w_2} w_{2i} + \sum_{s=1}^S z_{is}(\rho) u_s, \quad (3)$$

where w_{1i} and w_{2i} are the spatial coordinates with corresponding coefficients β_{w_1} and β_{w_2} , $z_{is}(\rho) = R_\rho(\mathbf{w}_i - \boldsymbol{\kappa}_s)$ and $\mathbf{u} = (u_1, u_2, \dots, u_S)^\top$ are assumed to be normally distributed such that $(\mathbf{u} | \lambda_{spat}, \rho) \sim \mathcal{N}_S(0, (\lambda_{spat} \Omega_\rho)^{-1})$, where $\lambda_{spat} > 0$ and $\Omega_\rho = R_\rho(\boldsymbol{\kappa}_s - \boldsymbol{\kappa}_{s'})$ is an $S \times S$ matrix for all $s, s' \in 1, \dots, S$. Here, $R_\rho(\cdot)$ is the covariance function used in kriging and $\boldsymbol{\kappa}_s$ ($s = 1, \dots, S$) is a subset of the spatial coordinates. One way to efficiently choose these two-dimensional knots ($\boldsymbol{\kappa}_s$) is through the use of a space-filling algorithm (Johnson et al., 1990; Nychka and Saltzman,

1998). In addition, there is an additional parameter, ρ , representing the range parameter in kriging, see e.g. Fahrmeir et al. (2013) pp. 453 - 456, for commonly used covariance functions. The covariance functions used in this paper are:

$$\text{Exponential : } R_\rho(\mathbf{d}) = \lambda_{spat}^{-1} \exp(-\rho\|\mathbf{d}\|),$$

$$\text{Matérn : } R_\rho(\mathbf{d}) = \lambda_{spat}^{-1} \exp(-\rho\|\mathbf{d}\|)(1 + \rho\|\mathbf{d}\|),$$

$$\text{Spherical : } R_\rho(\mathbf{d}) = \lambda_{spat}^{-1} (1 - 1.5\rho\|\mathbf{d}\| + 0.5\rho^3\|\mathbf{d}\|^3) \mathbb{I}(\|\mathbf{d}\| \leq \rho^{-1}),$$

$$\text{Circular : } R_\rho(\mathbf{d}) = \lambda_{spat}^{-1} \exp(-\rho^2\|\mathbf{d}\|^2),$$

where $\|\cdot\|$ refers to the Euclidean distance and $\mathbb{I}(\cdot)$ is the indicator function. In the Gaussian scenario, it becomes apparent that even without the inclusion of the additional error term as in (2), model (3) is capable of generating accurate predictions for $y_i(\mathbf{w}_i)$. This is primarily due to the fact that any extra variance introduced by ε tends to be absorbed by the measurement error variance inherent in the Gaussian model. However, the same cannot be said for count data when the Poisson distribution is assumed. To address this, we propose a negative binomial model for the count data. In this way, the error term ε is regarded as excess variability, which can be effectively managed by the overdispersion parameter in the negative binomial model. This allows for a more accurate estimation of the prediction uncertainty. However, if this excess variability is small, then the Poisson assumption may be sufficient. It is also important to note that equation (3) represents a model for the average spatial process.

2.2 Bayesian model formulation

For ease of notation let $y_i := y_i(\mathbf{w}_i)$. To generalize the derivations, we can write the probability distributions of y_i as an exponential dispersion family, $y_i \sim \text{EDF}(\gamma_i, \phi)$ with probability distribution given by $p(y_i; \gamma, \phi) = \exp\{[y_i\gamma_i - b(\gamma_i)]/a(\phi) + c(y_i, \phi)\}$ where ϕ is a dispersion parameter and γ_i is a natural parameter with mean $\mathbb{E}(y_i) = b'(\gamma_i) = \mu_i$ and variance $\mathbb{V}(y_i) = a(\phi)s''(\gamma_i)$.

The log-link function is used for the Poisson and negative binomial model such that $g(\mu_i) = \log(\mu_i)$. Note that an offset term N_i (e.g., number of populations) may be added so that $\mu_i = \exp(g(\mu_i)) \times N_i$. In matrix form, (1) can be written as:

$$\log(\boldsymbol{\mu}) = X\boldsymbol{\beta} + \sum_{j=1}^q B_j(s_j)\boldsymbol{\theta}_j + Z(\rho)\mathbf{u}, \quad (4)$$

where $\boldsymbol{\mu} = (\mu_1, \dots, \mu_n)^\top$, X is an $n \times (p + 3)$ matrix with i th row vector $\mathbf{x}_i = (1, x_{i1}, x_{i2}, \dots, x_{ip}, w_{1i}, w_{2i})^\top$ and coefficient vector $\boldsymbol{\beta} = (\beta_0, \beta_1, \beta_2, \dots, \beta_p, \beta_{w_1}, \beta_{w_2})^\top$, B_j is an $n \times K$ matrix with i th row $\mathbf{b}_{ij} = (b_{j1}(s_{ij}), b_{j2}(s_{ij}), \dots, b_{jK}(s_{ij}))^\top$ and coefficients $\boldsymbol{\theta}_j = (\theta_{j1}, \theta_{j2}, \dots, \theta_{jK})^\top$, $Z(\rho)$ is an $n \times S$ matrix with i th row $\mathbf{z}_i(\rho) = (z_{i1}(\rho), z_{i2}(\rho), \dots, z_{iS}(\rho))^\top$ and coefficients $\mathbf{u} = (u_1, u_2, \dots, u_S)^\top$ for $i = 1, \dots, n$ and $j = 1, \dots, q$.

A Gaussian prior is assumed for $\boldsymbol{\beta}$, i.e., $\boldsymbol{\beta} \sim \mathcal{N}_{\dim(\boldsymbol{\beta})}(0, V_\beta^{-1})$ where $V_\beta = \zeta I$ with small ζ (e.g. $\zeta = 10^{-5}$ in this paper). Denote the global design matrix as $C_\rho = [X : B_1 : B_2 : \dots : B_q : Z(\rho)]$ and the corresponding parameter vector $\boldsymbol{\xi} = (\boldsymbol{\beta}^\top, \boldsymbol{\theta}_1^\top, \dots, \boldsymbol{\theta}_q^\top, \mathbf{u}^\top)^\top$ such that equation (4) becomes $\log(\boldsymbol{\mu}) = C_\rho \boldsymbol{\xi}$. Moreover, let $\lambda_{spat} := \lambda_{q+1}$ and $\boldsymbol{\lambda} = (\lambda_1, \dots, \lambda_q, \lambda_{q+1})^\top$. Denote the precision of $\boldsymbol{\xi}$ by $Q_\xi^\lambda = \text{blkdiag}(V_\beta, \lambda_1 P, \dots, \lambda_q P, \lambda_{q+1} \Omega_\rho)$, where $\text{blkdiag}(\cdot)$ is a block diagonal matrix. The full Bayesian model is given by:

$$\begin{aligned} (y_i | \boldsymbol{\xi}) &\sim \text{EDF}(\gamma_i, \phi), \quad i = 1, \dots, n, \\ (\boldsymbol{\xi} | \boldsymbol{\lambda}, \rho) &\sim \mathcal{N}_{\dim(\boldsymbol{\xi})}(\mathbf{0}, (Q_\xi^\lambda)^{-1}), \\ (\lambda_j | \delta_j) &\sim \mathcal{G}\left(\frac{\nu}{2}, \frac{\nu \delta_j}{2}\right), \quad j = 1, \dots, q + 1, \\ \delta_j &\sim \mathcal{G}(a_\delta, b_\delta), \quad j = 1, \dots, q + 1, \\ p(\rho) &\propto \rho^{-1}, \\ p(\phi) &\propto \phi^{-1}, \end{aligned}$$

where $\mathcal{G}(a, b)$ denotes a Gamma distribution with mean a/b and variance a/b^2 . This robust prior specification on the penalty parameters follows from [Jullion and Lambert \(2007\)](#) where $a_\delta = b_\delta$ are chosen to be small enough, say 10^{-5} , with fixed ν (e.g. $\nu = 3$ in this paper).

2.3 Laplace approximation

This section discusses the derivations for the conditional posterior distribution of $\boldsymbol{\xi}$ and approximate posterior distributions of the hyperparameters. The Laplace approximation is used to approximate the conditional posterior $p(\boldsymbol{\xi}|\boldsymbol{\lambda}, \rho, \phi, \mathcal{D})$ as a Gaussian distribution. This posterior approximation is particularly advantageous for its computational efficiency, significantly reducing computational time, as it eliminates the need for sampling compared to MCMC methods. In the case of a Gaussian response, the derived conditional posterior is exactly Gaussian, and the detailed derivations are provided in Appendix A. Denote the (Poisson or negative binomial) likelihood function by $\mathcal{L}(\boldsymbol{\xi}, \rho, \phi; \mathcal{D})$ where \mathcal{D} is the observed data. Using Bayes' rule, the conditional posterior of $\boldsymbol{\xi}$ can be written as $p(\boldsymbol{\xi}|\boldsymbol{\lambda}, \rho, \phi, \mathcal{D}) \propto \mathcal{L}(\boldsymbol{\xi}, \rho, \phi; \mathcal{D})p(\boldsymbol{\xi}|\boldsymbol{\lambda}, \rho)$. The gradient and Hessian of the log-conditional posterior, $\log p(\boldsymbol{\xi}|\boldsymbol{\lambda}, \rho, \phi, \mathcal{D})$, with respect to $\boldsymbol{\xi}$ are analytically derived and used in a Newton-Raphson algorithm to approximate the mode of the conditional posterior of $\boldsymbol{\xi}$. The availability of the derived analytic gradient and Hessian further enhances the computational speed. After convergence, the Laplace approximation of $p(\boldsymbol{\xi}|\boldsymbol{\lambda}, \rho, \phi, \mathcal{D})$ is a multivariate Gaussian density denoted by $\tilde{p}_G(\boldsymbol{\xi}|\boldsymbol{\lambda}, \rho, \phi, \mathcal{D}) = \mathcal{N}_{\dim(\boldsymbol{\xi})}(\hat{\boldsymbol{\xi}}_{\boldsymbol{\lambda}}, \hat{\Sigma}_{\boldsymbol{\lambda}})$ where $\hat{\boldsymbol{\xi}}_{\boldsymbol{\lambda}}$ is the mode and $\hat{\Sigma}_{\boldsymbol{\lambda}}$ is the inverse of the negative Hessian matrix evaluated at the posterior mode.

Next, the (approximate) joint posterior distribution of the hyperparameters $\boldsymbol{\lambda}$, $\boldsymbol{\delta}$, ρ and ϕ is derived. Let $\boldsymbol{\delta} = (\delta_1, \delta_2, \dots, \delta_q)^\top$. Using Bayes' theorem, the joint marginal posterior of $\boldsymbol{\lambda}$, $\boldsymbol{\delta}$, ρ and ϕ can be written as:

$$p(\boldsymbol{\lambda}, \boldsymbol{\delta}, \rho, \phi|\mathcal{D}) \propto \frac{\mathcal{L}(\boldsymbol{\xi}, \rho, \phi; \mathcal{D})p(\boldsymbol{\xi}|\boldsymbol{\lambda})p(\boldsymbol{\lambda}|\boldsymbol{\delta})p(\boldsymbol{\delta})p(\rho)p(\phi)}{p(\boldsymbol{\xi}|\boldsymbol{\lambda}, \rho, \phi, \mathcal{D})}.$$

Following Rue et al. (2009), this joint posterior can be approximated by replacing the denominator $p(\boldsymbol{\xi}|\boldsymbol{\lambda}, \rho, \phi, \mathcal{D})$ with $\tilde{p}_G(\boldsymbol{\xi}|\boldsymbol{\lambda}, \rho, \phi, \mathcal{D})$ and by evaluating $\boldsymbol{\xi}$ at $\hat{\boldsymbol{\xi}}_{\boldsymbol{\lambda}}$. Note that the determinant $|Q_{\boldsymbol{\xi}}^{\boldsymbol{\lambda}}|^{\frac{1}{2}}$ in $p(\boldsymbol{\xi}|\boldsymbol{\lambda})$ can be obtained as $|Q_{\boldsymbol{\xi}}^{\boldsymbol{\lambda}}|^{\frac{1}{2}} = \left(|V_{\beta}| \times |\lambda_1 P| \times \dots \times |\lambda_q P| \times |\lambda_{q+1} \Omega_{\rho}| \right)^{\frac{1}{2}} \propto$

$(\lambda_1^K \times \dots \times \lambda_q^K \times \lambda_{q+1}^S |\Omega_\rho|)^{\frac{1}{2}}$. The approximate joint posterior can then be written as:

$$\begin{aligned} \tilde{p}(\boldsymbol{\lambda}, \boldsymbol{\delta}, \rho, \phi | \mathcal{D}) &\propto \mathcal{L}(\boldsymbol{\xi}, \rho, \phi; \mathcal{D}) \times \exp\left(-\frac{1}{2} \widehat{\boldsymbol{\xi}}_\lambda^\top Q \boldsymbol{\lambda} \widehat{\boldsymbol{\xi}}_\lambda\right) \times \prod_{j=1}^q (\lambda_j)^{\frac{K+\nu}{2}-1} \times \lambda_{q+1}^{\frac{S+\nu}{2}-1} \\ &\times \prod_{j=1}^{q+1} (\delta_j)^{\frac{\nu}{2}+a_\delta-1} \exp\left(-\left(\frac{\nu\lambda_j}{2} + b_\delta\right) \delta_j\right) \\ &\times |\Omega_\rho|^{\frac{1}{2}} \rho^{-1} \phi^{-1} |\widehat{\Sigma}_\lambda|^{\frac{1}{2}}. \end{aligned} \quad (5)$$

From (5), the joint posterior $\tilde{p}(\boldsymbol{\lambda}, \rho, \phi | \mathcal{D})$ can be analytically obtained by integrating out the hyperparameters δ_j . To ensure numerical stability, the remaining hyperparameters are log-transformed such that $\mathbf{v} = (v_1, \dots, v_{q+1})^\top = (\log(\lambda_1), \dots, \log(\lambda_{q+1}))^\top$, $v_\rho = \log(\rho)$ and $v_\phi = \log(\phi)$. Note that the transformed posterior is multiplied by the Jacobian of the transformation given by $J = \prod_{j=1}^{q+1} \exp(v_j) \times \exp(v_\rho) \times \exp(v_\phi)$. The joint log-posterior of \mathbf{v} , v_ρ and v_ϕ is then given by:

$$\begin{aligned} \log \tilde{p}(\mathbf{v}, v_\rho | \mathcal{D}) &\doteq \log \mathcal{L}(\boldsymbol{\xi}, v_\rho, v_\phi; \mathcal{D}) - 0.5 \widehat{\boldsymbol{\xi}}_v^\top Q \boldsymbol{\xi}^v \widehat{\boldsymbol{\xi}}_v + \sum_{j=1}^q \left(\frac{K+\nu}{2} v_j\right) + \left(\frac{S+\nu}{2} v_{q+1}\right) \\ &- \sum_{j=1}^{q+1} \left(\frac{\nu}{2} + a_\delta\right) \log\left(\frac{\nu \exp(v_j)}{2} + b_\delta\right) + \frac{1}{2} \log |\Omega_{v_\rho}| + \frac{1}{2} \log |\widehat{\Sigma}_v|, \end{aligned}$$

where \doteq denotes equality up to an additive constant. The above log-posterior is then optimized to obtain the maximum a posteriori estimate for \mathbf{v} , v_ρ and v_ϕ .

2.4 Prediction and prediction interval

The main goal of kriging is to predict the value of the response variable y_0 at an arbitrary location $\mathbf{w}_0 = (w_{1_0}, w_{2_0})^\top$. Suppose the linear and smooth covariates are available denoted by $(x_{1_0}, x_{2_0}, \dots, x_{p_0})$ and $(s_{1_0}, s_{2_0}, \dots, s_{q_0})$, respectively. Define $\mathbf{x}_0 = (1, x_{1_0}, x_{2_0}, \dots, x_{p_0}, w_{1_0}, w_{2_0})^\top$ and denote the B-spline basis for the smooth covariates by $\mathbf{b}_{j_0} = (b_{j_1}(s_{j_0}), b_{j_2}(s_{j_0}), \dots, b_{j_K}(s_{j_0}))^\top$ for $j = 1, \dots, q$. The spline basis for the coordinates is given by $\mathbf{z}_0(\hat{\rho}) = (z_{1_0}(\hat{\rho}), z_{2_0}(\hat{\rho}), \dots, z_{S_0}(\hat{\rho}))^\top$, where $z_{s_0}(\hat{\rho}) = R_{\hat{\rho}}(\mathbf{w}_0 - \boldsymbol{\kappa}_s)$ for $s = 1, \dots, S$ and $\hat{\rho}$ is the maximum a posteriori estimate of ρ . Furthermore, define

$\mathbf{c}_{\hat{\rho}} = (\mathbf{x}_0^\top, \mathbf{b}_{1_0}^\top, \mathbf{b}_{2_0}^\top, \dots, \mathbf{b}_{q_0}^\top, \mathbf{z}_0(\hat{\rho})^\top)^\top$. From model (4), the estimated mean response can be obtained as $\widehat{\mathbb{E}(y_0)} = \exp(\mathbf{c}_{\hat{\rho}}^\top \widehat{\boldsymbol{\xi}}_\lambda)$.

To obtain predictions, note that $\log(\mathbb{E}(y_0)) = \mathbf{c}_{\hat{\rho}}^\top \boldsymbol{\xi}$, where $\tilde{p}_G(\boldsymbol{\xi} | \mathbf{v}, v_\rho, v_\phi, \mathcal{D}) = \mathcal{N}_{\dim(\boldsymbol{\xi})}(\widehat{\boldsymbol{\xi}}_v, \widehat{\boldsymbol{\Sigma}}_v)$. The approximate posterior distribution for the log mean number of cases is thus $\tilde{p}(\log(\mathbb{E}(y_0)) | \mathbf{v}, v_\rho, v_\phi, \mathcal{D}) = \mathcal{N}_1(\mathbf{c}_{\hat{\rho}}^\top \widehat{\boldsymbol{\xi}}_v, \mathbf{c}_{\hat{\rho}}^\top \widehat{\boldsymbol{\Sigma}}_v \mathbf{c}_{\hat{\rho}})$. From this Gaussian distribution, 1000 samples are drawn with mean $\mathbf{c}_{\hat{\rho}}^\top \widehat{\boldsymbol{\xi}}_v$ and variance $\mathbf{c}_{\hat{\rho}}^\top \widehat{\boldsymbol{\Sigma}}_v \mathbf{c}_{\hat{\rho}}$. These samples are exponentiated to obtain an estimated mean vector, denoted by $\boldsymbol{\mu}_0$. Subsequently, 1000 samples are generated from a Poisson or negative binomial distribution with mean vector $\boldsymbol{\mu}_0$ to obtain predictive samples for y_0 . The corresponding quantiles of these samples are then computed to determine the desired prediction interval. Note that in the presence of an offset term N_i , both \widehat{y}_0 and $\boldsymbol{\mu}_0$ are multiplied by N_i .

2.5 Bayesian information criteria and test for smooth effects

The effective degrees of freedom (ED) serve as a measure of model complexity and quantify the amount of smoothing in a given model. A covariate with an associated ED value close to 1 indicates a linear effect, while values greater than 1 indicate nonlinearity. Let $\mathcal{I} = -\nabla_{\boldsymbol{\xi}}^2 \log \mathcal{L}(\boldsymbol{\xi}, \rho, \phi; \mathcal{D})|_{\boldsymbol{\xi}=\widehat{\boldsymbol{\xi}}_\lambda}$ denote the negative Hessian of the log-likelihood evaluated at the posterior mode estimate $\widehat{\boldsymbol{\xi}}_\lambda$. The total ED is computed by summing the main diagonal of the matrix $\mathcal{H} = \widehat{\boldsymbol{\Sigma}}_\lambda \mathcal{I}$, where $\widehat{\boldsymbol{\Sigma}}_\lambda$ is the estimated covariance matrix of $\boldsymbol{\xi}$. The ED of a specific smooth term is obtained by summing the diagonal elements of \mathcal{H} that correspond to the B-spline coefficients associated with the smooth term. The Bayesian information criteria (BIC) (Schwarz, 1978) is useful for model selection and is computed using the formula $BIC = -2 \log \mathcal{L}(\boldsymbol{\xi}, \rho, \phi; \mathcal{D}) + \text{ED} \times \log(n)$. A lower BIC indicates a better fit of the model.

Wood (2013) proposed a test statistic, T_r , to test the effect of a smooth covariate. T_r is a Wald-type statistic used to test the null hypothesis $H_0 : f_j(x) = 0$ versus the alternative hypothesis $H_a : f_j(x) \neq 0$ for a smooth covariate x . Let $\widehat{f}_j = B_j \widehat{\boldsymbol{\theta}}_j$ denote the estimated j th smooth function, where B_j and $\widehat{\boldsymbol{\theta}}_j$ are the associated B-spline matrix and estimated coefficients, respectively. The covariance matrix of \widehat{f}_j is given by $V_{\widehat{f}_j} = B_j \widehat{\boldsymbol{\Sigma}}_{\boldsymbol{\theta}_j} B_j^\top$, where $\widehat{\boldsymbol{\Sigma}}_{\boldsymbol{\theta}_j}$ is the estimated

covariance matrix of the B-spline coefficients θ_j . The test statistic is computed as $T_r = \widehat{f}_j^\top V_{\widehat{f}_j}^{r-} \widehat{f}_j$, where $V_{\widehat{f}_j}^{r-}$ is the rank- r Moore-Penrose inverse of $V_{\widehat{f}_j}$ and r is the estimated effective degrees of freedom for the j th smooth. Under the null hypothesis, T_r follows a Gamma distribution, that is $T_r \sim \mathcal{G}(r/2, 1/2)$, with mean $\mathbb{E}(T_r) = r$ and variance $\mathbb{V}(T_r) = 2r$.

3 Simulation study

A simulation study is conducted to evaluate the performance of our proposed methodology. For the count data, the samples y are generated from a Poisson distribution with rate parameter $\mu \cdot \exp(\varepsilon)$. The inclusion of $\exp(\varepsilon)$ preserves the stochasticity of the true spatial process in agreement with equation (2). Thus, this is equivalent to simulating a spatial component from a two-dimensional smooth function plus an error term ($s(w_1, w_2) + \varepsilon$). For the Gaussian data, ε represents the error term of the Gaussian distribution, such that observations y have mean μ and variance $\mathbb{V}(\varepsilon) = \sigma^2$. In the simulation, the following mean structure is assumed:

$$\mu = \beta_0 + \beta_1 x_1 + f(x_2) + s(w_1, w_2),$$

where $\beta_0 = 3$, $\beta_1 = -0.5$, and $f(x_2) = \cos(2\pi x_2)$. The covariates x_1 and x_2 are randomly simulated from a uniform distribution over the unit interval, and ε is drawn from a zero mean Gaussian distribution with standard deviation $\sigma = 0.25$ for the count data and $\sigma = \sqrt{0.10}$ for the Gaussian data. The spatial component $s(w_1, w_2)$ is a two-dimensional smooth function, for which the following three different forms are considered:

$$\begin{aligned} s_1(w_1, w_2) &= 0.5 - \frac{w_1^2 + w_2^2}{18}, \\ s_2(w_1, w_2) &= \frac{w_1^3 + w_1 w_2 + w_2^2}{25}, \\ s_3(w_1, w_2) &= -\frac{(w_1 - w_2)^2}{15} + \sin(w_1) \cos(w_2). \end{aligned}$$

Here, the spatial coordinates w_1 and w_2 are simulated from a uniform distribution on the interval $(-3, 3)$. The plot for the two-dimensional smooth functions considered in the simulation is shown in Figure 1.

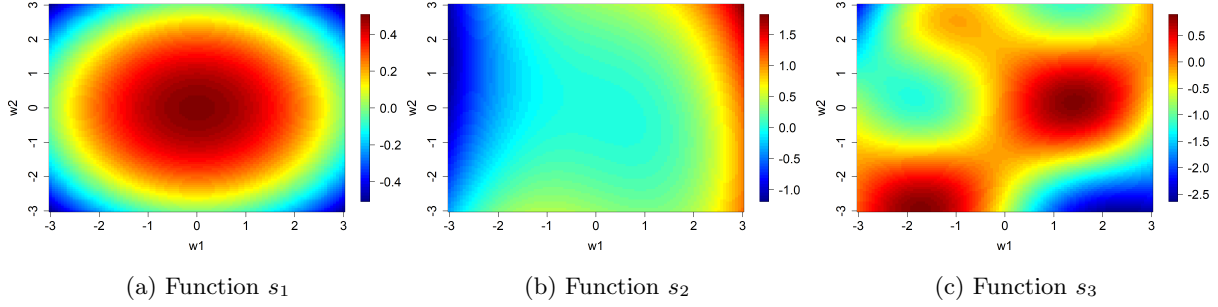


Figure 1: Two-dimensional smooth functions.

The performance measures used in our study are bias, relative bias (%Bias), and credible interval (CI) coverage. These measures are computed for μ , the smooth term $f(x_2)$, and the spatial term $s(w_1, w_2)$. Additionally, the prediction interval (PI) coverage for the samples y are calculated. For smooth and spatial terms, a grid of values for x_2 and a two-dimensional grid for (w_1, w_2) are created. Using these grids, $f(x_2)$ and $s(w_1, w_2)$ are computed, and the corresponding relative bias and PI coverage are obtained. To avoid identifiability issues, column mean centering is imposed for the basis functions associated with the smooth and spatial components and the performance measures are computed on the mean centered $f(x_2)$ and $s(w_1, w_2)$. Due to this centering, the bias is only computed for μ . Suppose that the quantity of interest is denoted by ω with the corresponding estimate $\hat{\omega}$. The bias and relative bias are computed as follows:

$$\text{Bias} = \frac{1}{B \times M} \sum_{b=1}^B \sum_{m=1}^M (\omega_{bm} - \hat{\omega}_{bm}),$$

$$\% \text{Bias} = \frac{1}{B \times M} \sum_{b=1}^B \sum_{m=1}^M \left| \frac{\omega_{bm} - \hat{\omega}_{bm}}{\omega_{bm}} \right| \times 100\%,$$

where M is the length of the grid created for the covariates, and B is the number of simulations or generated realizations. Moreover, CI or PI coverage is determined by calculating the percentage of ω values that fall within the interval.

Tables 1-3 present the results for different functions (s_1 , s_2 and s_3) across various covariance structures (circular, exponential, Matérn, and spherical) and different model distributions (neg-

ative binomial, Poisson, and Gaussian). The percentage bias for the smooth term is around 4% to 7% for all scenarios (Tables 1-3), demonstrating low bias and suggesting robust performance in estimating smooth effects using our proposed method. For all functions (s_1, s_2 and s_3), the negative binomial model has coverage rates of the smooth term that are generally closer to the 95% nominal level for the smooth term as compared to the Poisson model which shows undercoverage, with rates ranging from 73% to 80%. The Gaussian data, on the other hand, also demonstrates good coverage, ranging from 91% to 94%, which is slightly lower than the nominal level. Note that the relative bias for the Gaussian data is very low, around 4% to 5%.

Regarding the spatial term, the Gaussian model generally exhibits the lowest relative bias, followed by the negative binomial model, while the Poisson model has the highest bias. Notably, all covariance functions show similar relative biases across each model for the spatial term, except for the Matérn covariance function. For the Poisson model, the Matérn covariance consistently shows lower bias. In the negative binomial and Gaussian models, the Matérn covariance has a relatively low bias for function s_1 but a higher bias for functions s_2 and s_3 . The coverage for the spatial term is highest for the negative binomial model, ranging from 97% to 99%, except for the Matérn covariance, which has lower coverage for functions s_2 and s_3 , with rates of 83% and 69%, respectively. This pattern is similar to the Gaussian data, with coverage mostly close to the 95% nominal level, although there is undercoverage for the Matérn covariance for functions s_2 and s_3 . This behavior for the spatial term suggests that using our proposed model, the Matérn covariance might be more suitable for symmetric functions (s_1) but not for non-symmetric functions in modeling the spatial component. On the other hand, the other covariance functions are more robust regardless of the shape of the underlying spatial structure. Finally, the Poisson model shows undercoverage for all functions and covariance structures.

For the mean response, biases are generally close to zero for all scenarios, with the percentage bias being lowest for the Gaussian data, ranging between 1% to 3%, except for the Matérn covariance with function s_3 , where the relative bias is around 6%. The relative bias for μ is mostly lower for the negative binomial model compared to the Poisson model, but their values are very similar, ranging around 4% to 9%, except for function s_3 with the Matérn covariance

in the negative binomial model, which has a relative bias of 13%. Finally, for the response y , the Gaussian model has prediction interval coverage very close to the nominal level. For count data, the Poisson model shows undercoverage, while the negative binomial model has high prediction interval coverage. Overall, the negative binomial and Gaussian models demonstrate robust performance, characterized by low bias and high coverage rates across all quantities of interest. In contrast, although the Poisson model exhibits low bias, it suffers from lower coverage rates due to the presence of an additional error term, treated as an overdispersion parameter, that is unaccounted for within the Poisson model.

Additional simulation results without covariates are presented in Appendix B, comparing the proposed model with the classical kriging approach for the Gaussian data using the `geoR` package, yielding comparable results, although the low-rank approach has a slightly larger percentage bias in terms of the mean. Moreover, the computation time is compared using the `microbenchmark()` function from the `microbenchmark` package in R with 10 functions evaluated for 1000 observations. The analysis is implemented on a device with an Intel(R) Core(TM) i5-1135G7, CPU running at a base frequency of 2.40GHz, and having 4 cores with 16GB of RAM. The average real elapsed time for the proposed Bayesian approach is around 1 second, while the classical kriging approach takes around 110 seconds on average (see Table B.2 in the Appendix). This highlights the computational benefit of our methodology.

Table 1: Simulation results for function s_1 . Model - distributional assumption for the response. Covariance - covariance functions used in modeling the spatial component. CP(%) - indicates 95% interval coverage probability.

Model	Covariance	Smooth term $f(x_2)$		Spatial term $s(w_1, w_2)$		μ		y
		Bias(%)	CP(%)	Bias(%)	CP(%)	Bias	Bias (%)	CP(%)
Negative binomial	Circular	5.49	94.08	23.43	99.43	-0.96	5.42	98.11
	Exponential	5.41	93.94	22.95	98.99	-1.09	5.39	98.16
	Matérn	5.40	93.66	17.77	98.36	-0.86	4.71	98.10
	Spherical	5.32	93.62	23.24	99.25	-1.00	5.38	98.10
Poisson	Circular	5.92	76.84	39.35	80.73	-0.91	7.57	83.00
	Exponential	5.80	76.39	38.20	80.83	-0.99	7.36	82.74
	Matérn	5.52	77.37	19.20	77.93	-0.95	5.19	82.75
	Spherical	5.98	76.46	39.99	80.63	-0.93	7.65	83.33
Gaussian	Circular	4.88	92.34	19.87	97.77	-0.02	1.49	94.42
	Exponential	4.92	92.42	21.01	96.73	-0.02	1.55	94.38
	Matérn	4.81	91.74	16.21	95.04	-0.01	1.26	94.77
	Spherical	4.88	92.26	20.06	97.49	-0.02	1.49	94.46

Table 2: Simulation results for function s_2 . Model - distributional assumption for the response. Covariance - covariance functions used in modeling the spatial component. CP(%) - indicates 95% interval coverage probability.

Model	Covariance	Smooth term $f(x_2)$		Spatial term $s(w_1, w_2)$		μ		y
		Bias(%)	CP(%)	Bias(%)	CP(%)	Bias	Bias (%)	CP(%)
Negative binomial	Circular	5.53	93.78	18.51	97.43	0.37	6.49	97.90
	Exponential	5.62	92.53	18.44	97.36	0.51	6.62	97.88
	Matérn	5.43	94.12	20.60	83.10	0.38	7.06	98.02
	Spherical	5.47	94.11	18.90	97.97	0.20	6.52	97.90
Poisson	Circular	5.82	76.46	27.88	80.23	-0.41	7.89	82.09
	Exponential	5.89	76.12	27.01	80.38	-0.18	7.68	81.72
	Matérn	5.99	73.84	15.94	75.44	-0.48	5.99	81.31
	Spherical	6.35	73.98	28.58	79.93	-0.40	8.01	81.92
Gaussian	Circular	4.89	92.48	16.78	94.76	0.00	1.94	94.37
	Exponential	4.99	92.84	16.87	93.59	0.00	1.98	94.28
	Matérn	4.84	92.61	26.34	52.35	0.00	2.59	94.66
	Spherical	4.92	92.60	16.69	94.41	0.00	1.93	94.38

Table 3: Simulation results for function s_3 . Model - distributional assumption for the response. Covariance - covariance functions used in modeling the spatial component. CP(%) - indicates 95% interval coverage probability.

Model	Covariance	Smooth term $f(x_2)$		Spatial term $s(w_1, w_2)$		μ		y
		Bias(%)	CP(%)	Bias(%)	CP(%)	Bias	Bias (%)	CP(%)
Negative binomial	Circular	6.06	93.95	13.44	97.16	-0.34	8.05	98.15
	Exponential	5.83	94.62	13.60	97.17	-0.33	8.03	98.25
	Matérn	7.31	91.99	19.86	69.01	-0.20	13.09	99.15
	Spherical	5.95	94.93	13.28	97.60	-0.34	7.97	98.26
Poisson	Circular	6.51	79.43	15.82	83.74	-0.53	8.92	87.19
	Exponential	6.46	79.82	15.84	82.86	-0.51	9.03	87.29
	Matérn	6.22	78.44	12.75	70.28	-0.64	8.26	86.65
	Spherical	6.28	79.42	15.85	83.77	-0.45	8.98	87.36
Gaussian	Circular	5.01	92.66	11.10	95.28	-0.01	2.85	94.70
	Exponential	4.97	92.41	11.24	94.76	-0.02	2.87	94.64
	Matérn	5.32	94.14	22.74	44.49	-0.02	5.91	96.31
	Spherical	5.00	93.25	11.23	95.17	-0.02	2.87	94.55

4 Data application

In this section, the proposed methodology is applied to the analysis of two datasets: (1) Meuse river data using the Gaussian model and (2) vulnerability to coronavirus disease 2019 (COVID-19) in Belgium using the negative binomial model.

4.1 Meuse river data

The Meuse dataset contains measurements of heavy metal concentrations in topsoil collected from the flood plain of the Meuse River near the village of Stein, Netherlands. It also includes the geographic coordinates of each sampling location and is commonly used to demonstrate kriging and other geostatistical techniques. This analysis focuses on zinc concentrations in the topsoil, using two covariates: (1) distance to the Meuse river (dist), and (2) relative elevation above the local riverbed (elev). The dataset is available in the R package `sp`.

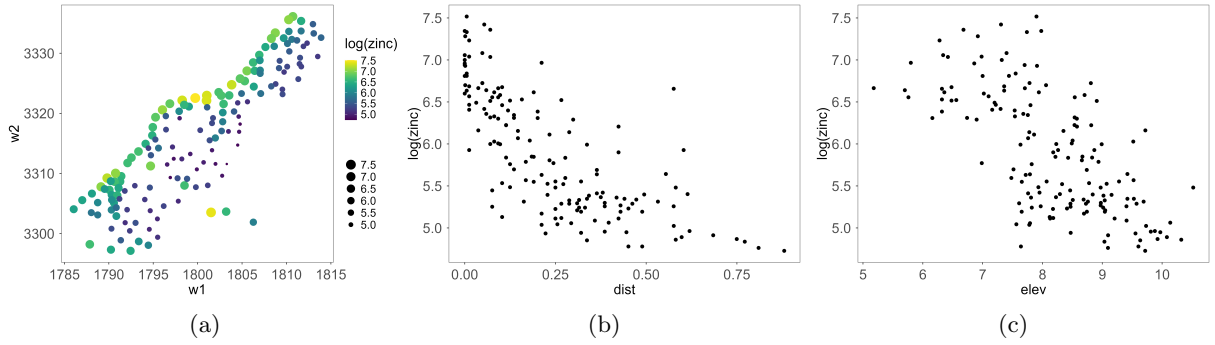


Figure 2: (a) Observed log-zinc values over the sampling locations (w_1, w_2) ; (b) Scatterplot of observed log-zinc with the covariate distance; (c) Scatterplot of observed log-zinc with the covariate elevation.

Figure 2 displays the observed logarithm of zinc ($\log\text{-zinc}$) values at sampling locations (w_1, w_2) and scatter plots illustrating the relationship between $\log\text{-zinc}$ and the variables, distance, and elevation. The data indicates nonlinearity between distance and $\log\text{-zinc}$ values, whereas elevation suggests linearity. Classical geostatistical methods typically accommodate only the linear effects of covariates. Therefore, transformation is commonly applied (e.g. a square root transformation of distance) in order to fit a linear geostatistical model. One benefit of our proposed method is the direct incorporation of nonlinear covariates without the need for any transformation. The distance and elevation are included as smooth covariates, using a Gaussian model for the $\log\text{-zinc}$, with various covariance structures. Table 4 shows that the BIC values are similar for different model covariances, with the Circular covariance having the lowest BIC. Consequently, the model using circular covariance is examined further. Both tests for the significance of the two smooth covariates yield a $p\text{-value} < 0.0001$, indicating a statistically significant relationship between the covariates and $\log\text{-zinc}$. Since Figure 2c indicates a linear effect of elevation, a model is fitted with elevation as a linear covariate, resulting in a BIC of -126.89, higher than the BIC (-128.94) obtained when elevation is included as a smooth covariate. Therefore, the final model includes both distance and elevation as smooth covariates given by:

$$\log(\text{zinc}_i) = \beta_0 + f(\text{dist}_i) + f(\text{elev}_i) + s(w_{1i}, w_{2i}) + \epsilon_i, \quad (6)$$

for $i = 1, \dots, 155$. Figure 3 presents the estimated effects of the covariates. Figure 4 shows the

estimated spatial surface and the comparison between fitted and observed log-zinc values based on model (6).

Table 4: Results for Gaussian model fitted on Meuse river data.

Covariance	BIC
Circular	-128.94
Exponential	-128.12
Matérn	-126.61
Spherical	-127.14

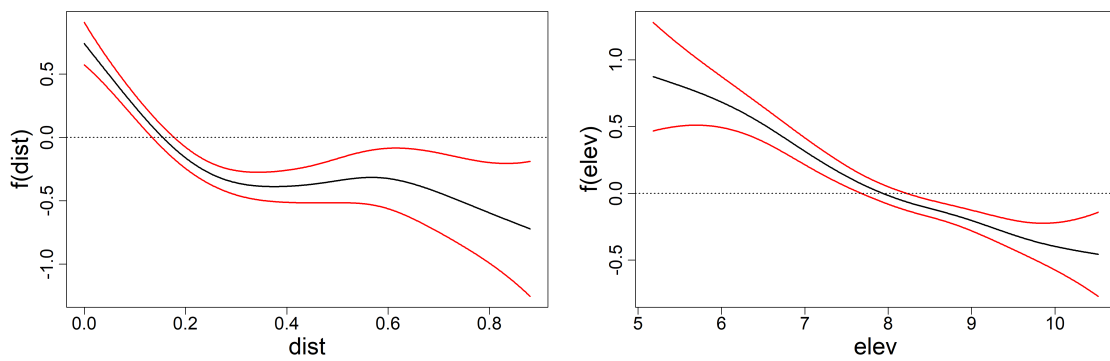


Figure 3: Estimated effects of smooth covariates on log-zinc.

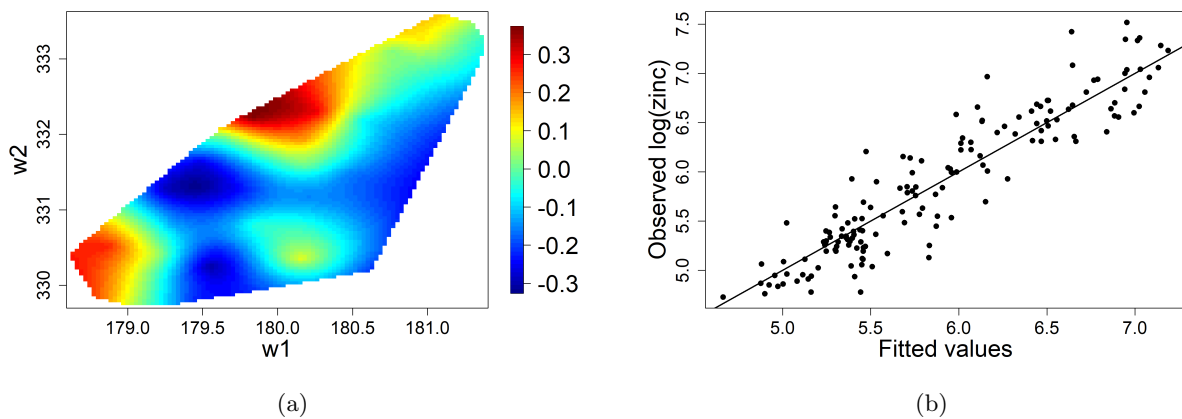


Figure 4: Results for the Meuse data using model (6). (a) Estimated continuous surface for the spatial term $s(w_1, w_2)$; (b) Estimated mean vs observed log-zinc values.

4.2 COVID-19 vulnerability data

The proposed negative binomial model is applied to the analysis of the COVID-19 data from Flanders and Brussels regions in Belgium from September 1, 2020, to December 31, 2020. The study area is divided into 9627 statistical sectors, each with a population ranging from a minimum of 7 to a maximum of 6082, with an average population of approximately 740 inhabitants. The population per 100 inhabitants of each statistical sector is used as an offset term in the model. The centroid of each statistical sector serves as the coordinate for the spatial analysis. The dataset includes the number of positive cases and various risk factors for each statistical sector. Variables identified in the literature as risk factors for vulnerability to COVID-19 are considered. Correlations between these variables are then examined, with only one variable retained from each pair that had an absolute Pearson correlation greater than 0.5. The final factors include median net income (*med_inc*) (Rozenfeld et al., 2020; Wachtler et al., 2020), the proportion of retired people (*pensinr*) (Rozenfeld et al., 2020; Pijls et al., 2021), the proportion of non-Belgian residents (*nonBel*) (Hayward et al., 2021), the proportion of single parents (Sung, 2021) (*snglprn*), the yearly average black carbon level (*bc*) (Rozenfeld et al., 2020; Wu et al., 2020), and the proportion of females (*female*) (Wu and Qian, 2022). All these variables are standardized.

Initially, all factors are considered as smooth covariates. Various covariance functions are fitted with the spherical covariance having the lowest BIC, as shown in Table 5. Therefore, further data analysis is conducted using spherical covariance, showing that all factors have statistically significant effects (p-value < 0.0001). The plot illustrating the estimated smooth effects is shown in Figure C.2 in the Appendix. To investigate the linear effects, each smooth covariate is subsequently replaced as a linear covariate, and the BIC is compared to that of the full model (BIC = 1221406), where all factors are smooth covariates. As shown in Table 6, the factors *med_inc* and *bc* resulted in lower BIC when included as linear covariates rather than smooth covariates.

Table 5: BIC results for the negative binomial model fitted on COVID-19 data using different covariance functions.

Covariance	BIC
Circular	-1221386
Exponential	-1221397
Matérn	-1221187
Spherical	-1221406

Table 6: BIC comparison for the COVID-19 data using spherical covariance when the variables are added as linear covariates.

Variables	BIC with linear covariate	Difference from BIC with smooth covariate
med_inc	-1221420	-14
pensinr	-1221388	18
nonBel	-1221403	3
snglprn	-1221351	55
bc	-1221422	-16
female	-1221388	18

Therefore, the final model is given by:

$$\log(\mu_i) = \beta_0 + \beta_1 med_inc_i + \beta_2 bc_i + f(pensinr_i) + f(nonBel_i) + f(sngplrn_i) + f(female_i) + s(w_{1i}, w_{2i}) + \log(N_i), \quad (7)$$

where N_i is the offset term per 100 population for $i = 1, \dots, 9627$. The estimated coefficients for the linear covariates in Table 7 indicate that areas with higher median net income are negatively correlated with the number of COVID-19 cases, while areas with high levels of black carbon are positively correlated with the number of cases. Table 8 shows the results for the nonlinear covariates in model (7) and the plot of the estimated smooth effects is shown in Figure 5. The latter figure shows that areas with higher proportions of pensioners and single parents exhibit higher vulnerability to COVID-19 compared to the average. However, areas with average or lower proportions of these groups correspond to average vulnerability. For the covariate *pensinr*, the smooth trend for higher values shows a wider credible interval, indicating higher uncertainty in the trend direction, which could potentially go up or down. This is due to the limited number of observations (only five) for *pensinr* values greater than 5. Other covariates also show higher

uncertainty at the right tail because of the few observations, which are right-skewed (see Figure C.1 in the Appendix). Areas with higher proportions of non-Belgians and lower proportions of females appear to be less vulnerable to COVID-19. Finally, the plot for the estimated spatial surface and the comparison between fitted and observed cases is shown in Figure 6.

Table 7: Results for the linear covariates in model 7. Estimate - estimated coefficient; SE - standard error; CI lower - 95% lower credible interval; CI upper - 95% upper credible interval.

Variables	Estimate	SE	CI lower	CI upper
(Intercept)	1.180	0.005	1.170	1.190
med_inc	-0.073	0.007	-0.088	-0.059
bc	0.047	0.010	0.028	0.066

Table 8: Results for the smooth covariates in model 7.

Variables	ED	T_r	p-value
pensinr	5.10	37.95	< 0.0001
nonBel	4.92	26.27	< 0.0001
snglprn	5.87	45.68	< 0.0001
female	3.43	63.86	< 0.0001

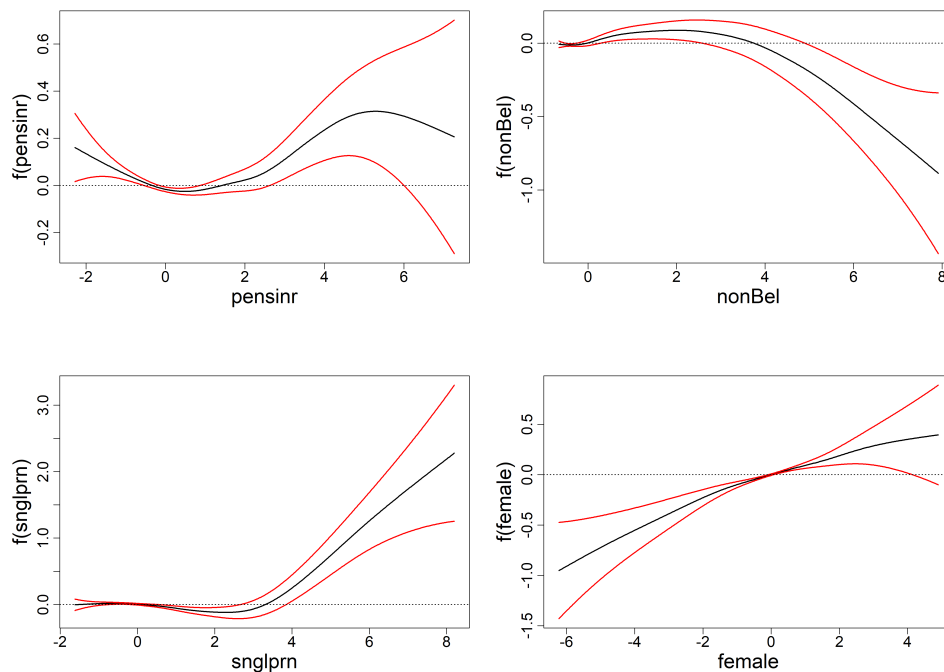
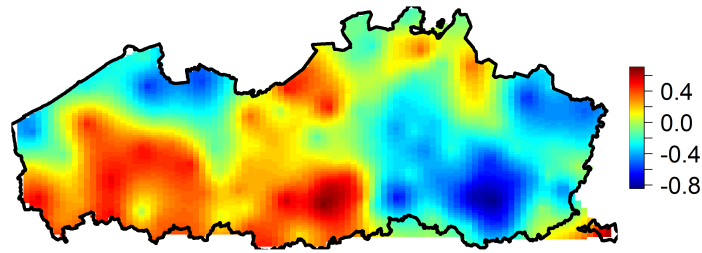
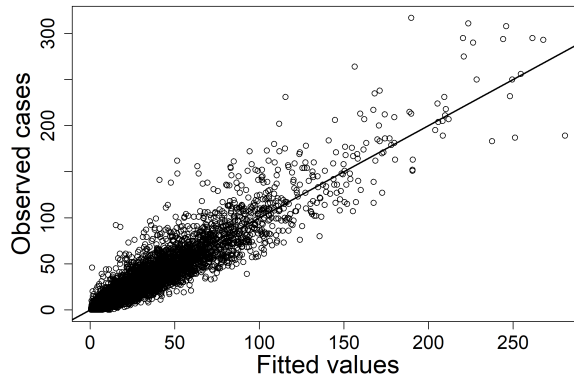


Figure 5: Estimated effects of smooth covariates for COVID-19 data using spherical covariance.



(a)



(b)

Figure 6: Results for the COVID-19 data using model (7). (a) Estimated continuous surface for the spatial term $s(w_1, w_2)$ overlaying the map of the study region; (b) Estimated mean vs observed number of COVID-19 positive cases.

5 Conclusion

This paper presents a novel Bayesian method for geostatistical modeling that combines Laplace approximations, P-splines, and low-rank representations for spatial processes. The proposed model offers several advantages, including the ability to perform spatial interpolation and investigate the effects of both linear and nonlinear covariates. Its computational efficiency is substantially improved by using Laplace approximations and a low-rank representation of the spatial process, leading to faster computation times. Additionally, the model extends beyond Gaussian responses to accommodate Poisson and negative binomial models, thereby providing robust options for handling count data. Thus, the proposed approach not only enhances the flexibility and speed of geostatistical analyses but also broadens their applicability across

different types of data.

Simulation studies demonstrate that the proposed model exhibits low relative bias and has credible intervals close to the nominal coverage with respect to the underlying target smooth function and spatial process. These results are consistent across all covariance functions, except for the Matérn covariance, which did not perform well in terms of credible interval coverage for the spatial component in non-symmetric two-dimensional functions. Additionally, the proposed model demonstrates good predictive interval coverage across all covariance functions, highlighting its robust predictive ability. In the presence of overdispersion, the Poisson model, as expected, results in undercoverage, but the availability of the negative binomial model within our proposed framework effectively addresses this issue.

The proposed model has been applied to the Meuse river data and COVID-19 vulnerability data in Belgium, demonstrating its practical applicability. The analysis of COVID-19 data reveals that areas with lower median incomes are more vulnerable to the virus, highlighting the economic disparities exacerbated by the pandemic (Rozenfeld et al., 2020; Wachtler et al., 2020). Additionally, areas with a higher proportion of pensioners who are at increased risk for severe COVID-19 outcomes show higher vulnerability (Rozenfeld et al., 2020; Pijls et al., 2021). Environmental factors, such as higher levels of black carbon, further contribute to increased susceptibility, underscoring how air pollution contributes to health disparities (Rozenfeld et al., 2020; Wu et al., 2020). Social demographics also play a significant role, for instance, areas with higher proportions of females (Wu and Qian, 2022) and single parents (Sung, 2021) are more vulnerable to the virus. Interestingly, while studies indicate that migrants are generally at high risk for COVID-19 (Hayward et al., 2021), our findings suggest that areas with a high proportion of non-Belgians are less vulnerable to the disease.

Finally, an interesting extension of our proposed model is to assume a binomial distribution for the count response, considering the population size. This could enhance model performance in scenarios such as disease prevalence modeling, where count data naturally follows a binomial distribution due to the presence of binary outcomes (e.g. disease vs. no disease) within a given

population size.

Competing Interest Statement

The authors have declared no competing interest.

References

- Cressie, N. (1993). *Statistics for Spatial Data*. John Wiley & Sons.
- Cressie, N., Sainsbury-Dale, M., and Zammit-Mangion, A. (2022). Basis-function models in spatial statistics. *Annual Review of Statistics and Its Application*, 9:373–400.
- Diggle, P. J. and Giorgi, E. (2019). *Model-Based Geostatistics for Global Public Health: Methods and Applications*. Chapman and Hall/CRC.
- Eilers, P. H. C. and Marx, B. D. (1996). Flexible smoothing with B-splines and penalties. *Statistical Science*, 11(2):89–121.
- Fahrmeir, L., Kneib, T., Lang, S., and Marx, B. (2013). *Regression Models*. Springer.
- Gressani, O. and Lambert, P. (2021). Laplace approximations for fast Bayesian inference in generalized additive models based on P-splines. *Computational Statistics & Data Analysis*, 154:107088.
- Hayward, S. E., Deal, A., Cheng, C., Crawshaw, A., Orcutt, M., Vandrevalla, T. F., Norredam, M., Carballo, M., Ciftci, Y., Requena-Méndez, A., et al. (2021). Clinical outcomes and risk factors for COVID-19 among migrant populations in high-income countries: a systematic review. *Journal of Migration and Health*, 3:100041.
- Johnson, M. E., Moore, L. M., and Ylvisaker, D. (1990). Minimax and maximin distance designs. *Journal of Statistical Planning and Inference*, 26(2):131–148.
- Jullion, A. and Lambert, P. (2007). Robust specification of the roughness penalty prior distribution in spatially adaptive Bayesian P-splines models. *Computational Statistics & Data Analysis*, 51(5):2542–2558.
- Kammann, E. and Wand, M. P. (2003). Geoadditive models. *Journal of the Royal Statistical Society Series C: Applied Statistics*, 52(1):1–18.
- Lang, S. and Brezger, A. (2004). Bayesian P-splines. *Journal of Computational and Graphical Statistics*, 13(1):183–212.

- Nychka, D. and Saltzman, N. (1998). Design of air-quality monitoring networks. In *Case studies in environmental statistics*, volume 132, pages 51–76. Springer.
- Pijls, B. G., Jolani, S., Atherley, A., Derckx, R. T., Dijkstra, J. I. R., Franssen, G. H. L., Hendriks, S., Richters, A., Venemans-Jellema, A., Zalpuri, S., et al. (2021). Demographic risk factors for COVID-19 infection, severity, ICU admission and death: a meta-analysis of 59 studies. *BMJ Open*, 11(1):e044640.
- Rozenfeld, Y., Beam, J., Maier, H., Haggerson, W., Boudreau, K., Carlson, J., and Medows, R. (2020). A model of disparities: risk factors associated with COVID-19 infection. *International Journal for Equity in Health*, 19(1):126.
- Rue, H., Martino, S., and Chopin, N. (2009). Approximate Bayesian inference for latent Gaussian models by using integrated nested Laplace approximations. *Journal of the Royal Statistical Society: Series B (Statistical Methodology)*, 71(2):319–392.
- Ruppert, D., Wand, M. P., and Carroll, R. J. (2003). *Semiparametric regression*. Number 12. Cambridge University Press.
- Schwarz, G. (1978). Estimating the dimension of a model. *The Annals of Statistics*, 6(2):461–464.
- Sung, B. (2021). A spatial analysis of the association between social vulnerability and the cumulative number of confirmed deaths from COVID-19 in United States counties through November 14, 2020. *Osong Public Health and Research Perspectives*, 12(3):149.
- Vandendijck, Y., Faes, C., and Hens, N. (2017). Estimating the spatial covariance structure using the geoadditive model. *Environmental and Ecological Statistics*, 24:341–361.
- Wachtler, B., Michalski, N., Nowossadeck, E., Diercke, M., Wahrendorf, M., Santos-Hövenner, C., Lampert, T., and Hoebel, J. (2020). Socioeconomic inequalities and COVID-19—A review of the current international literature. *Journal of Health Monitoring*, 5(Suppl 7):3.
- Waller, L. A. and Gotway, C. A. (2004). *Applied Spatial Statistics for Public Health Data*. John Wiley & Sons.
- Wand, M. P. (2003). Smoothing and mixed models. *Computational Statistics*, 18:223–249.

- Wikle, C. K. (2010a). Hierarchical modeling with spatial data. *Handbook of Spatial Statistics*, pages 89–106.
- Wikle, C. K. (2010b). Low-rank representations for spatial processes. *Handbook of Spatial Statistics*, 107:118.
- Wood, S. N. (2013). On p-values for smooth components of an extended generalized additive model. *Biometrika*, 100(1):221–228.
- Wood, S. N. (2017). *Generalized additive models: an introduction with R*. Chapman and Hall/CRC.
- Wu, C. and Qian, Y. (2022). The gender peak effect: Women are most vulnerable to infections during COVID-19 peaks. *Frontiers in Public Health*, 10:937179.
- Wu, X., Nethery, R. C., Sabath, M. B., Braun, D., and Dominici, F. (2020). Exposure to air pollution and covid-19 mortality in the United States: A nationwide cross-sectional study. *MedRxiv*, pages 2020–04.
- Zimmerman, D. L. (2010). Likelihood-based methods. *Handbook of Spatial Statistics*, pages 45–56.
- Zimmerman, D. L. and Stein, M. (2010). Classical geostatistical methods. *Handbook of Spatial Statistics*, pages 29–44.

Appendix

A. Derivations for the Gaussian case

Assuming a Gaussian distribution on the observations $y_i(\mathbf{w}_i)$, we have the following geoaddivitive model:

$$y_i(\mathbf{w}_i) = \beta_0 + \beta_1 x_{i1} + \cdots + \beta_p x_{ip} + f_1(s_{i1}) + \cdots + f_q(s_{iq}) + s(\mathbf{w}_i) + \epsilon_i, \quad \epsilon_i \sim \mathcal{N}_1(0, \tau_\epsilon^{-1}).$$

The full Bayesian model for the Gaussian case is given by:

$$\begin{aligned} (\mathbf{y}|\boldsymbol{\xi}) &\sim \mathcal{N}_n(C_\rho \boldsymbol{\xi}, \tau_\epsilon^{-1} I) \\ (\boldsymbol{\xi}|\boldsymbol{\lambda}, \tau_\epsilon, \rho) &\sim \mathcal{N}_{\dim(\boldsymbol{\xi})}(\mathbf{0}, (\tau_\epsilon Q_\xi^\lambda)^{-1}), \\ (\lambda_j|\delta_j) &\sim \mathcal{G}\left(\frac{\nu}{2}, \frac{\nu \delta_j}{2}\right), \quad j = 1, \dots, q+1, \\ \delta_j &\sim \mathcal{G}(a_\delta, b_\delta), \quad j = 1, \dots, q+1, \\ p(\tau_\epsilon) &\propto \frac{1}{\tau_\epsilon}, \\ p(\rho) &\propto \frac{1}{\rho}. \end{aligned}$$

The conditional posterior of $\boldsymbol{\xi}$ can be written as:

$$\begin{aligned} p(\boldsymbol{\xi}|\boldsymbol{\lambda}, \tau_\epsilon, \rho, \mathcal{D}) &\propto \mathcal{L}(\boldsymbol{\xi}, \tau_\epsilon, \rho|\mathcal{D}) \times p(\boldsymbol{\xi}|\boldsymbol{\lambda}, \tau_\epsilon, \rho) \\ &\propto \exp(-0.5\tau_\epsilon \|\mathbf{y} - C_\rho \boldsymbol{\xi}\|^2) \times \exp(-0.5\tau_\epsilon \boldsymbol{\xi}^\top Q_\xi^\lambda \boldsymbol{\xi}). \end{aligned}$$

It can be shown that $p(\boldsymbol{\xi}|\boldsymbol{\lambda}, \tau_\epsilon, \rho, \mathcal{D}) \propto \exp\left(0.5\boldsymbol{\xi} \widehat{\Sigma}_\lambda^{-1} \boldsymbol{\xi} - 2\boldsymbol{\xi} \widehat{\Sigma}_\lambda^{-1} \widehat{\boldsymbol{\xi}}_\lambda\right)$, where $\widehat{\boldsymbol{\xi}}_\lambda = (C_\rho^\top C_\rho + Q_\xi^\lambda)^{-1} C_\rho^\top \mathbf{y}$ and $\widehat{\Sigma}_\lambda = \tau_\epsilon^{-1} (C_\rho^\top C_\rho + Q_\xi^\lambda)^{-1}$. This can be recognized as proportional to a multivariate Gaussian distribution with mean vector $\widehat{\boldsymbol{\xi}}_\lambda$ and covariance matrix $\widehat{\Sigma}_\lambda$. Therefore, the conditional posterior of $\boldsymbol{\xi}$ is a Gaussian density given by $(\boldsymbol{\xi}|\boldsymbol{\lambda}, \tau_\epsilon, \rho, \mathcal{D}) \sim \mathcal{N}_{\dim(\boldsymbol{\xi})}(\widehat{\boldsymbol{\xi}}_\lambda, \widehat{\Sigma}_\lambda)$.

Posterior distribution of hyperparameters

Using Bayes' theorem, the marginal joint posterior of hyperparameters $\boldsymbol{\lambda}$, τ_ϵ and ρ is given by:

$$p(\boldsymbol{\lambda}, \tau_\epsilon, \rho | \mathcal{D}) \propto \frac{\mathcal{L}(\boldsymbol{\xi}, \tau_\epsilon, \rho; \mathcal{D}) p(\boldsymbol{\xi} | \boldsymbol{\lambda}, \tau_\epsilon, \rho) p(\boldsymbol{\lambda} | \boldsymbol{\delta}) p(\tau_\epsilon) p(\rho)}{p(\boldsymbol{\xi} | \boldsymbol{\lambda}, \tau_\epsilon, \rho, \mathcal{D})}.$$

The above posterior can be approximated by evaluating $\boldsymbol{\xi}$ at the mode $\widehat{\boldsymbol{\xi}}_\lambda$. Note also that $|Q_\xi^\lambda| = |V_\beta| \times |\lambda_1 P| \times \cdots \times |\lambda_q P| \times |\lambda_{q+1} \Omega_\rho| \propto \lambda_1^K \times \cdots \times \lambda_q^K \times \lambda_{q+1}^S |\Omega_\rho|$. Hence, the approximated marginal posterior of the hyperparameter is given by

$$\begin{aligned} \tilde{p}(\boldsymbol{\lambda}, \tau_\epsilon, \rho | \mathcal{D}) &\propto \tau_\epsilon^{\frac{n}{2}} \exp\left(-0.5\tau_\epsilon \|\mathbf{y} - C_\rho \widehat{\boldsymbol{\xi}}_\lambda\|^2\right) \times \tau_\epsilon^{\frac{\dim(\widehat{\boldsymbol{\xi}}_\lambda)}{2}} |Q_\xi^\lambda|^{\frac{1}{2}} \exp(-0.5\tau_\epsilon \widehat{\boldsymbol{\xi}}_\lambda^\top Q_\xi^\lambda \widehat{\boldsymbol{\xi}}_\lambda) \\ &\times \prod_{j=1}^{q+1} (\delta_j)^{\frac{\nu}{2}} (\lambda_j)^{\frac{\nu}{2}-1} \exp\left(-\frac{\nu\delta_j}{2} \lambda_j\right) \times \prod_{j=1}^{q+1} (\delta_j)^{a_\delta-1} \exp(-b_\delta \delta_j) \\ &\times \frac{1}{\tau_\epsilon} \times \frac{1}{\rho} \times |\widehat{\boldsymbol{\Sigma}}_\lambda|^{\frac{1}{2}} \times \tau_\epsilon^{-\frac{\dim(\widehat{\boldsymbol{\xi}}_\lambda)}{2}} |C_\rho^\top C_\rho + Q_\xi^\lambda|^{-\frac{1}{2}} \\ &= \tau_\epsilon^{\frac{n}{2}-1} \exp\left(-0.5\tau_\epsilon (\|\mathbf{y} - C_\rho \widehat{\boldsymbol{\xi}}_\lambda\|^2 + \widehat{\boldsymbol{\xi}}_\lambda^\top Q_\xi^\lambda \widehat{\boldsymbol{\xi}}_\lambda)\right) \times \prod_{j=1}^q (\lambda_j)^{\frac{K+\nu}{2}-1} (\lambda_{q+1})^{\frac{S+\nu}{2}-1} \\ &\times \frac{1}{\rho} |\Omega_\rho|^{-\frac{1}{2}} |C_\rho^\top C_\rho + Q_\xi^\lambda|^{-\frac{1}{2}} \prod_{j=1}^{q+1} (\delta_j)^{\frac{\nu}{2}+a_\delta-1} \exp\left(-\left(\frac{\nu\lambda_j}{2} + b_\delta\right) \delta_j\right). \quad \text{Eq. (A.1)} \end{aligned}$$

The terms in the last line involving τ_ϵ and δ_j can be recognized as a kernel of a gamma density.

Thus, integrating $\tilde{p}(\boldsymbol{\lambda}, \tau_\epsilon, \rho | \mathcal{D})$ successively with respect to τ_ϵ and δ_j for $j = 1, \dots, q+1$ yields

$$\begin{aligned} \tilde{p}(\boldsymbol{\lambda}, \rho | \mathcal{D}) &\propto (\|\mathbf{y} - C_\rho \widehat{\boldsymbol{\xi}}_\lambda\|^2 + \widehat{\boldsymbol{\xi}}_\lambda^\top Q_\xi^\lambda \widehat{\boldsymbol{\xi}}_\lambda)^{-\frac{n}{2}} \times \rho^{-1} |\Omega_\rho|^{\frac{1}{2}} \times |C_\rho^\top C_\rho + Q|^{-\frac{1}{2}} \\ &\times \prod_{j=1}^q (\lambda_j)^{\frac{K+\nu}{2}-1} (\lambda_{q+1})^{\frac{S+\nu}{2}-1} \times \prod_{j=1}^{q+1} \left(\frac{\nu\lambda_j}{2} + b_\delta\right)^{-\frac{\nu}{2}+a_\delta}. \end{aligned}$$

Let $\mathbf{v} = (v_1, \dots, v_{q+1})^\top = (\log(\lambda_1), \dots, \log(\lambda_{q+1}))^\top$ and $v_\rho = \log(\rho)$. Using the method of transformation, the Jacobian of the transformation is given by $J = \exp(v_\rho) \prod_{j=1}^{q+1} \exp(v_j)$. Then the joint posterior of \mathbf{v} and v_ρ is given by

$$\begin{aligned} \tilde{p}(\mathbf{v}, v_\rho | D) &\propto (\|\mathbf{y} - C_{v_\rho} \hat{\boldsymbol{\xi}}_\lambda\|^2 + \hat{\boldsymbol{\xi}}_\lambda^\top Q_\xi^\lambda \hat{\boldsymbol{\xi}}_\lambda)^{-\frac{n}{2}} \times |\Omega_{v_\rho}|^{\frac{1}{2}} \times |C_{v_\rho}^\top C_{v_\rho} + Q_\xi^\lambda|^{-\frac{1}{2}} \\ &\times \prod_{j=1}^q (\exp(v_j))^{\frac{K+\nu}{2}} (\exp(v_{q+1}))^{\frac{S+\nu}{2}} \times \prod_{j=1}^{q+1} \left(\frac{\nu \exp(v_j)}{2} + b_\delta \right)^{-\frac{\nu}{2} + a_\delta}. \end{aligned}$$

Moreover, the log-posterior of v and v_ρ is

$$\begin{aligned} \log(\tilde{p}(\mathbf{v}, v_\rho | D)) &\doteq -\frac{n}{2} \log(\|\mathbf{y} - C_{v_\rho} \hat{\boldsymbol{\xi}}_\lambda\|^2 + \hat{\boldsymbol{\xi}}_\lambda^\top Q_\xi^\lambda \hat{\boldsymbol{\xi}}_\lambda) + \frac{1}{2} \log |\Omega_{v_\rho}| - \frac{1}{2} \log |C_{v_\rho}^\top C_{v_\rho} + Q_\xi^\lambda| \\ &+ \sum_{j=1}^q \left(\frac{K+\nu}{2} v_j \right) + \left(\frac{S+\nu}{2} v_{q+1} \right) - \sum_{j=1}^{q+1} \left(\frac{\nu}{2} + a_\delta \right) \log \left(\frac{\nu \exp(v_j)}{2} + b_\delta \right). \end{aligned}$$

Furthermore, from Eq. (A.1), the posterior of τ_ϵ conditional on $\boldsymbol{\lambda}$ and ρ is a gamma density given by $(\tau_\epsilon | \boldsymbol{\lambda}, \rho, D) \sim \mathcal{G} \left(\frac{n}{2}, 0.5(\|\mathbf{y} - C_\rho \hat{\boldsymbol{\xi}}_\lambda\|^2 + \hat{\boldsymbol{\xi}}_\lambda^\top Q_\xi^\lambda \hat{\boldsymbol{\xi}}_\lambda) \right)$.

B. Simulation study comparing the proposed model with the classical kriging approach

The proposed model for the Gaussian data is compared with the classical kriging approach using the `likfit()` function in the R package `geoR`. A model with constant mean and spatial term only is assumed for this simulation scenario. Specifically, the observations are generated from the model $y = \mu + \epsilon$, where $\mu = \beta_0 + s(w_1, w_2)$, $\beta_0 = 3$, $\epsilon \sim \mathcal{N}(0, \sqrt{0.10})$. The spatial term $s(w_1, w_2)$ is simulated from a Gaussian Random Field (GRF) using the `grf()` function in R with zero mean and different forms of covariances (circular, exponential, Matérn, spherical), with sill parameter $\lambda_{\text{spat}}^{-1} = 0.5$, and range parameter $\rho^{-1} = 0.15$. Results are presented in Table A.1.

Table B.1: Results comparing the proposed low-rank Gaussian model and the classical kriging approach with spatial component only. \mathcal{M}_1 - proposed method; \mathcal{M}_2 - using `likfit()` function in R.

	μ				y	
	Bias		(%Bias)		PI Coverage	
	\mathcal{M}_1	\mathcal{M}_2	\mathcal{M}_1	\mathcal{M}_2	\mathcal{M}_1	\mathcal{M}_2
Circular	-0.0061	0.0037	10.90	7.43	95.81	94.98
Exponential	-0.0039	0.0043	8.58	6.61	95.75	95.14
Matérn	-0.0023	0.0011	5.70	2.49	96.04	95.09
Spherical	-0.0067	0.0039	11.72	7.81	95.62	95.02

Table B.2: Comparison of computation time (in seconds) with 10 evaluations for Gaussian data without covariates.

	Min	Mean	Median	Max
Proposed method	0.87	1.03	0.98	1.57
Classical kriging approach (<code>likfit()</code>)	108.19	109.82	109.48	112.80

C. Additional results for the data applications

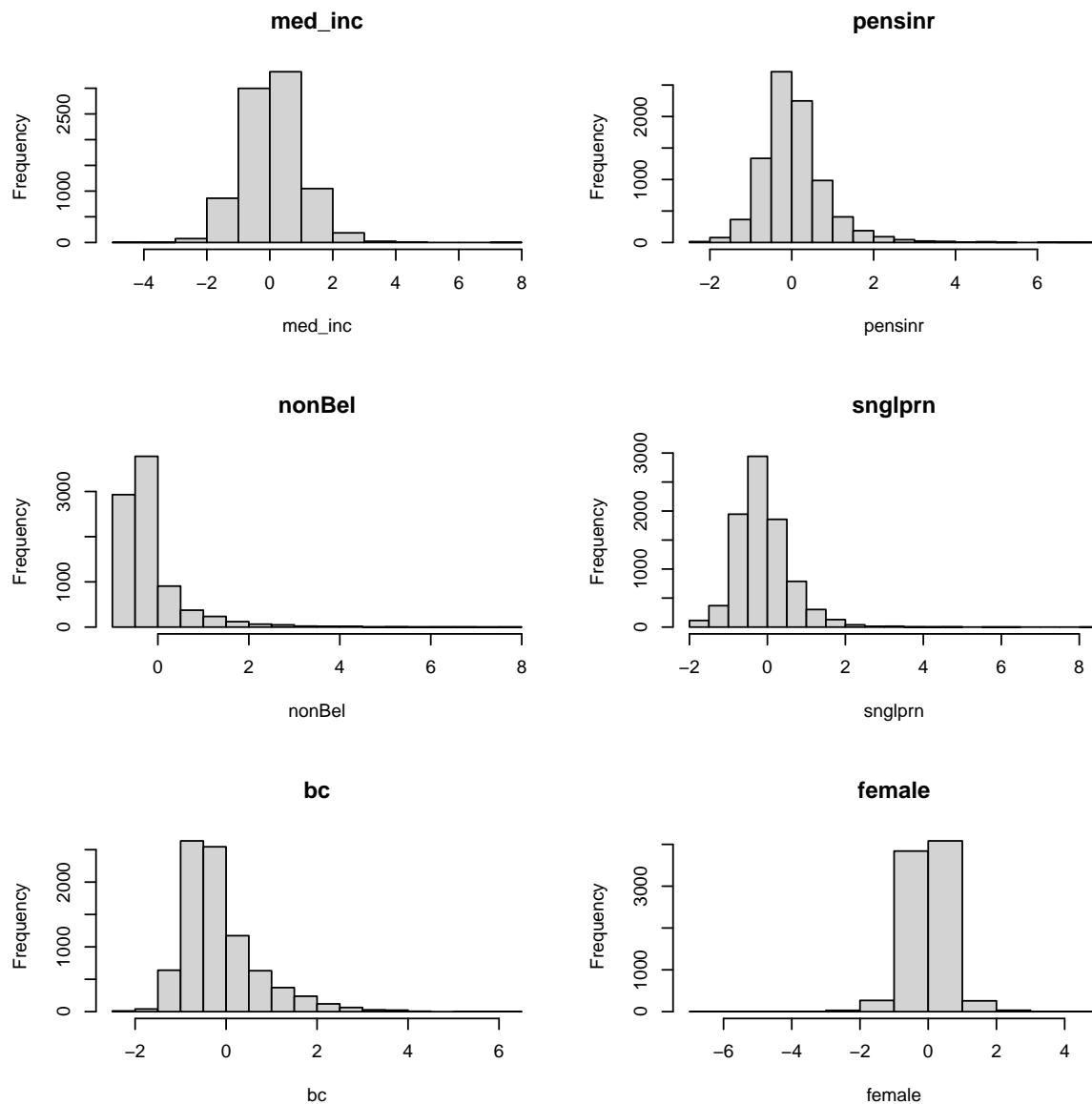


Figure C.1: Histogram of the factors considered in the analysis of COVID-19 data.

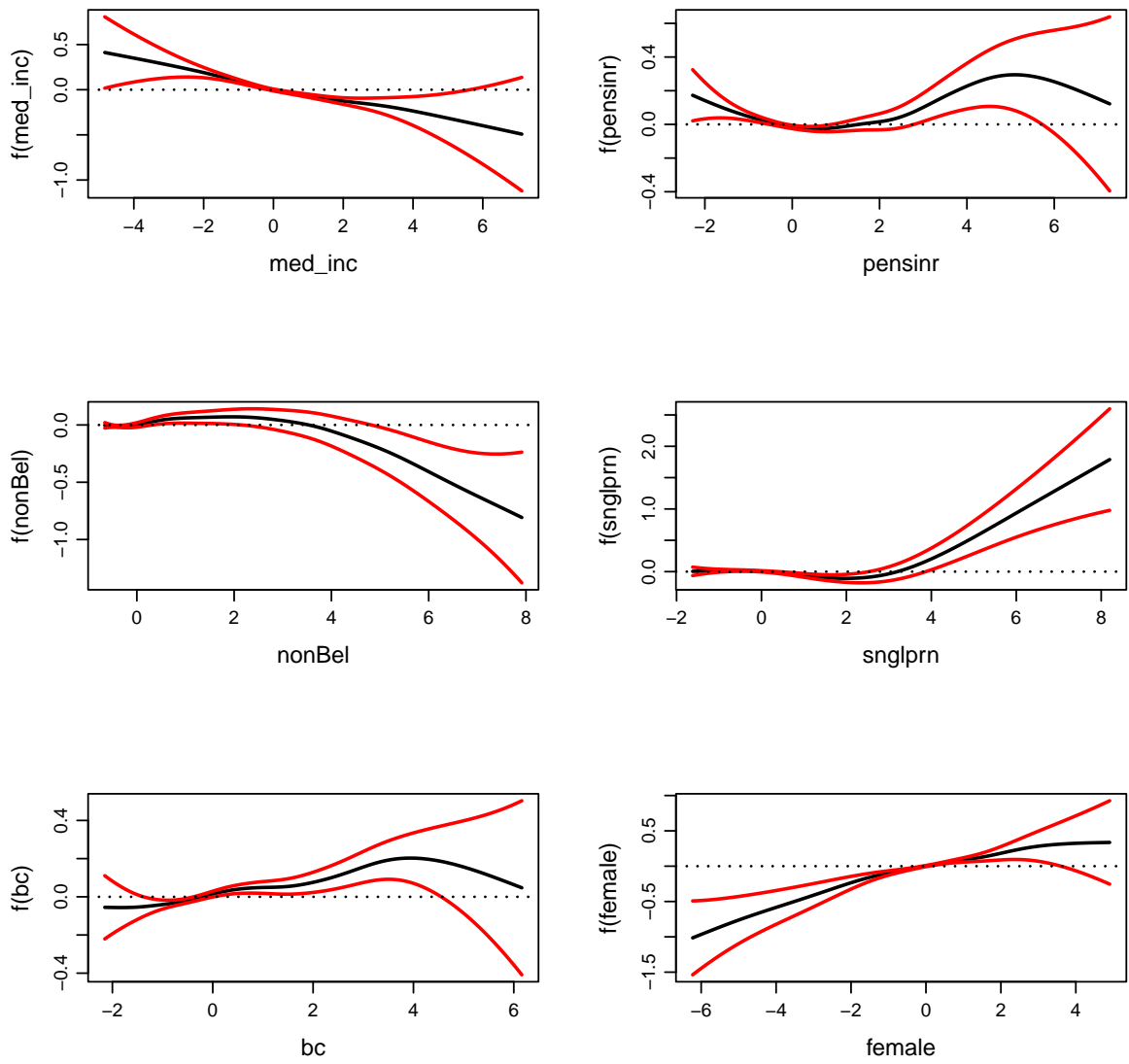


Figure C.2: Estimated smooth effects for the COVID-19 data using spherical covariance.